Received: 29 November 2018 | Revised: 25 March 2019 | Accepted: 27 March 2019 | Published on: 24 April 2019

DOI: 10.1002/qj.3538

INCOMPASS SPECIAL COLLECTION

Quarterly Journal of the Royal Meteorological Society RMetS

A case-study of land–atmosphere coupling during monsoon onset in northern India

Emma J. Barton[1] | Christopher M. Taylor[1] | Douglas J. Parker[2] | Andrew G. Turner[3,4] | Danijel Belušić[1,5] | Steven J. Böing[2] | Jennifer K. Brooke[6] | R. Chawn Harlow[6] | Phil P. Harris[1] | Kieran Hunt[3] | A. Jayakumar[7] | Ashis K. Mitra[7]

[1]Hydro-Climate Risks, Centre for Ecology and Hydrology, Wallingford, UK

[2]Institute for Climate and Atmospheric Science, School of Earth and Environment, University of Leeds, Leeds, UK

[3]Department of Meteorology, University of Reading, Reading, UK

[4]National Centre for Atmospheric Science, University of Reading, Reading, UK

[5]Rossby Centre, SMHI, Norrköping, Sweden

[6]Met Office, Exeter, Devon, UK

[7]NCMRWF, Noida, India

Correspondence
Emma J. Barton, Centre for Ecology and Hydrology, Wallingford, OX10 8BB, UK.
Email: emmbar@ceh.ac.uk

Funding information
Met Office; Ministry of Earth Sciences; Natural Environment Research Council, NE/L013819/1, NE/L013840/1, NE/L013843/1, NE/L01386X/1, NE/P003117/1; Royal Society; Wolfson Foundation

Abstract

This article presents a land–atmosphere case-study for a single day during monsoon onset, incorporating data from a research aircraft, satellite products and model outputs. The unique aircraft observations reveal temperature and humidity contrasts of up to 5 K and 4 g/kg in the planetary boundary layer induced by spatial variations in soil moisture. Both antecedent rain and irrigation were found to be drivers of this atmospheric variability. There is also evidence of soil moisture-induced mesoscale circulations above some surfaces. This is the first time such responses have been observed *in situ* over India. Soil moisture-driven temperature anomalies are larger than those found in previous observational studies in the African Sahel. Moreover, irrigation in the region is extensive, unlike in the Sahel, and has a similar atmospheric effect to antecedent rainfall. This implies that historical changes in irrigation practices are likely to have had an important influence on mesoscale processes within the Indian monsoon. We also examine evidence linking soil moisture and cloud formation. Above wetter soils we observed a suppression of shallow cloud, whilst the initiation of deep convection occurred mostly in areas affected by wet–dry soil moisture boundaries. To investigate the impact of soil moisture heterogeneity on large-scale wind flow, three model depictions of the day are assessed: the European Centre for Medium-Range Weather Forecasts ERA-Interim and ERA5 reanalyses, and a high-resolution (1.5 km) simulation generated using the Indian National Centre for Medium Range Weather Forecasting regional convection-permitting Unified Model. We find evidence indicating surface flux uncertainties in the models lead to ~3.5 hPa anomalies in the monsoon trough. This does affect the simulation of monsoon circulation and rainfall. Better representation of mesoscale land–atmosphere coupling is likely to improve the depiction of convection within weather and climate models over India.

KEYWORDS

aircraft observations, convection, Indian monsoon, irrigation, land–atmosphere coupling, monsoon trough, planetary boundary layer, soil moisture

1 | INTRODUCTION

The Indian monsoon supplies around 80% of the country's annual rainfall between June and September (Jain and Kumar, 2012; Bollasina, 2014). Society is very sensitive to monsoon variations on a variety of time-scales, particularly in the agricultural sector (Turner and Annamalai, 2012; Bollasina, 2014). Despite this, the monsoon is often poorly represented in general circulation models (GCMs) and forecasting remains a challenge (Sperber *et al.,* 2013).

Northern India has been considered a region of strong coupling between the land and atmosphere since the first results from the Global Land–Atmosphere Coupling Experiment (GLACE) were reported by Koster *et al.* (2004), based on an ensemble of land–atmosphere GCMs. Later findings, based on a combination of models and observations, are consistent with this assessment (e.g. Zhang *et al.,* 2008; Ferguson *et al.,* 2012). Northern India is also one of the most well-equipped regions in the world for irrigation (FAO, 2014). As a result, not only is rainfall being recycled back into the atmosphere but water is being added through pumping of deep groundwater stores (Douglas *et al.,* 2009). The influence of land–atmosphere interactions on monsoon circulation specific to India is therefore an important consideration for understanding and forecasting the Indian summer monsoon.

Feedbacks between soil moisture and precipitation have been shown from observations in several regions of the world (e.g. Findell *et al.,* 2011; Taylor *et al.,* 2011; 2012; Tuttle and Salvucci, 2016). In the context of a monsoon regime both observational (e.g. Taylor *et al.,* 2010; 2011) and modelling (e.g. Gaertner *et al.,* 2010; Gantner and Kalthoff, 2010; Rochetin *et al.,* 2017) studies have shown how antecedent rainfall patterns affect new storms in the Sahel. Convective storms create heterogeneous wet soil features that influence surface sensible and latent heat fluxes in subsequent days, particularly when vegetation cover is sparse (Lohou *et al.,* 2014). These variations in soil moisture can induce temperature and humidity gradients in the planetary boundary layer (PBL), and drive daytime mesoscale circulations (Mahrt *et al.,* 1994; Taylor *et al.,* 2007). These circulations provide a favourable environment for convective initiation (Garcia-Carreras *et al.,* 2010; Taylor *et al.,* 2010).

For the Indian monsoon region, modelling studies have discussed the impact of the land surface on simulations, with potential implications for the forecasting of monsoon rain (e.g. Niyogi *et al.,* 2007; Asharaf *et al.,* 2012; Kar *et al.,* 2014; Osuri *et al.,* 2017). For example, the modelling of deep convection can be improved through better representation of soil moisture and soil temperature (Osuri *et al.,* 2017) and the choice of land surface parametrization scheme can strongly influence monthly mean precipitation (Kar *et al.,* 2014). In recent decades, irrigated cropland has become an increasingly important component of the Indian land surface, particularly in the northern plains. This includes the introduction of additional water to the surface from groundwater pumping. Agricultural intensification can influence mesoscale convection and rainfall patterns (Douglas *et al.,* 2009) and has been linked to the weakening of monsoon rainfall since the 1950s (Paul *et al.,* 2016).

Observational studies in India (e.g. Goel and Srivastava, 1990; Joseph and Sijikumar, 2004; Monhan and Rao, 2012; Sandeep *et al.,* 2014) have looked at PBL characteristics during the monsoon season, in particular the differences between active (wet) and break (dry) spells. Soil moisture–atmosphere interaction could explain the observed contrasts (Sandeep *et al.,* 2014). However a comprehensive description of the land–atmosphere feedbacks that shape the Indian summer monsoon, and their relative impacts, is still lacking (Xue and Dirmeyer, 2015; Parker *et al.,* 2016).

During June and July 2016, the Interaction of Convective Organisation and Monsoon Precipitation, Atmosphere, Surface and Sea (INCOMPASS) project (Turner *et al.,* 2020) directed the first detachment of the UK Facility for Airborne Atmospheric Measurements (FAAM) BAe-146 research aircraft to India. The aim of the detachment was to provide an observational characterization of the atmosphere and its links to land and ocean conditions during the early stages of the monsoon. Here we present a case-study from the aircraft campaign, which focuses on a transect over the northern plains of India. The aim of the flight was to sample the PBL above areas of contrasting land use and rainfall history, particularly irrigated and non-irrigated regions. We also perform a model intercomparison, considering two reanalysis products and a high-resolution convection-permitting simulation, to examine large-scale impacts of soil moisture which are difficult to observe.

In the next section we describe the datasets employed in our observational and model-based analyses. The synoptic and land surface conditions on 30 June 2016, the day of the flight, are also described. In section 3 we present our analysis of soil moisture impact on the PBL and monsoon circulation based on observational and model data. Then we detail our analysis of the impact of soil moisture gradients on convection based on satellite observations (section 4). This is followed by a discussion in section 5 and a list of our main conclusions in section 6.

2 | DATA AND CONDITIONS ON 30 JUNE 2016

2.1 | Flight B968 and instruments used

This case-study concerns a low-level transect of flight B968 on 30 June 2016, covering just under 700 km from the semi-arid region of Rajasthan, eastwards around Jaipur and into the irrigated state of Uttar Pradesh (Figure 1).

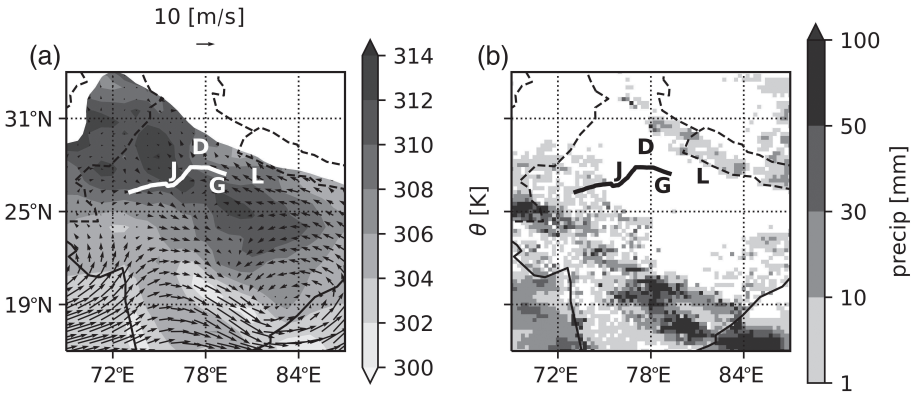

FIGURE 1 Low-level transect of INCOMPASS flight B968 on 30 June 2016 (thick solid line). (a) Potential temperature, θ (K), and wind vectors (m/s) plotted from ERA-Interim at 925 hPa and 0600 UTC. (b) 24 h accumulated precipitation, precip. (mm), up to 0300 UTC (0830 hr) on 30 June 2016, derived from composite precipitation dataset IMD-NCMRWF (Mitra *et al.,* 2013). The locations of Jaipur (J), Delhi (D), Gwalior (G) and Lucknow (L) are included for reference

The aircraft took measurements at a height of 190 m above ground level along the transect. The use of dropsondes was not permitted on this flight. The transect was performed between 1100 and 1230 hr (0530–0700 UTC; local time is UTC + 5.5 h) in order to sample the PBL prior to the development of deep convection. Solar noon is 1230 hr at Jaipur, near the centre of the transect. For full details of flight B968 and other flights in the INCOMPASS field campaign, see Turner *et al.* (2020).

Measurements from several instruments mounted on the aircraft were used in this case-study. Temperature, pressure and three-dimensional wind observations were recorded at 32 Hz. The horizontal wind vectors, and aircraft heading, are used to calculate along-track wind. A Water Vapor Sensing System version two (WVSSII) hygrometer provided water vapour measurement linearly interpolated to 1 Hz, from which specific humidity is derived. Vertical turbulent heat flux at the level of the flight is estimated from the 32 Hz temperature and vertical wind. Deviations in temperature and vertical wind velocity are determined with respect to a 150 s average (calculated using a Savitzky–Golay filter with third-order polynomials) whilst the flux is computed about a 300-second running mean of the product of the deviations. Changes in surface brightness temperature at 4 Hz directly below the aircraft were recorded using a Heimann radiometer. The readings from this instrument saturated above 328 K (approximately 55 °C), and therefore became unusable beyond that point, but still provide useful quantitative information on surface heterogeneity. For comparison, all these aircraft variables are averaged to the same temporal resolution of 1 s. Skin temperatures were also retrieved from Airborne Research Interferometer Evaluation System (ARIES) measurements. These ARIES surface temperatures are retrieved from low-level flight data using measurements on the downwelling and upwelling radiances in the 8–12 μm window region, along with temperature and humidity profile estimates from ERA-Interim.

2.2 | Satellite data

A number of satellite products are used to qualitatively interpret surface properties at the time of the flight. Brightness temperatures from the 10.7 GHz channel on board the Global Precipitation Mission (GPM, Level 1C product gridded at 13 km: GPM, 2014) are used to calculate Polarization Ratio (PR) in the region of the flight from an overpass at 0400 UTC. PR is a well-established proxy for surface wetness, and is the difference over the sum of horizontally and vertically polarized brightness temperatures. This proxy is used to locate areas of increased soil moisture and vegetation moisture content. Available data from existing soil moisture products is not used because these products either did not provide a suitably timed overpass prior to the flight, or did not have sufficient spatial coverage of the region of interest. Soil moisture and vegetation status is also inferred from MODerate-resolution Imaging Spectroradiometer (MODIS) Collection 6 Level 2 1 km resolution Land Surface Temperature (LST: Wan *et al.,* 2015) from the Terra overpass at 0500 UTC/1030 hr on 30 June 2016 and MODIS 8-day 1 km resolution Leaf Area Index (LAI, 25 June–2 July 2016: Myneni *et al.,* 2015). It should be noted that a Level 3 product is available for LST, but it contains almost no data for the time and region of interest. This is due to cloud screening, which appears to be over-conservative when compared with in-flight cloud observations, the MODIS true colour image, and other datasets (e.g. PR). Nonetheless, we note a significant discrepancy between the satellite LSTs and equivalent variables derived from on-board instruments. Rainfall history in the region of the flight is assessed based on a composite 1° gridded precipitation dataset (IMD-NCMRWF: Mitra *et al.,* 2013), produced from a combination of Integrated Multi-satellitE Retrievals for GPM (IMERG) and rain-gauge data. Finally, half-hourly Meteosat-7 (M7) data (~6 km resolution at this location, available from https://eoportal.

eumetsat.int/) are used to study local convective cloud development, in conjunction with MODIS true colour satellite imagery from the Terra and Aqua overpasses (available from https://worldview.earthdata.nasa.gov/).

2.3 | Model data

To investigate the large-scale impact of the surface on the PBL, three model depictions of 30 June 2016 are analysed. A regional model configuration of the Indian National Centre for Medium Range Weather Forecasting Unified Model (NCUM: Jayakumar *et al.,* 2017) was used to set up the high-resolution simulation over a domain covering the region of the flight (20.5–34.5°N, 69.6–83.5°E) at a horizontal grid length of 1.5 km. The model uses 80 vertical levels with a top at 38.5 km and 14 model levels below 1 km. The model time step is 60 s and the simulation was run for 72 h from an initial condition at 0000 UTC 29 June 2016. The initial and lateral boundary conditions are supplied by the current operational 17 km NCUM global model (Rakhi *et al.,* 2016). The cloud scheme is a regional version of the prognostic cloud fraction and condensate scheme based on Wilson *et al.* (2008). Convection in the regional model is considered resolvable and the subgrid-scale deep convection is not parametrized. The subgrid turbulence scheme used is the blended scheme (Boutle *et al.,* 2014) using a mixing factor of 0.5. Indian Space Research Organisation land-use land cover at 30 m resolution provides recent information about the vegetative and non-vegetative model tiles over the Indian region. Orography is derived from the NASA Shuttle Radar Topographic Mission 90 m digital elevation map. Further details of the 1.5 km NCUM model are given in Jayakumar *et al.* (2017).

For comparison with the high-resolution simulation, temperature and wind data from the European Centre for Medium-range Weather Forecasts (ECMWF) reanalyses ERA-Interim (Dee *et al.,* 2011) and new product ERA5 (Hersbach and Dee, 2016) at 925 hPa and 0600 UTC are employed. These data are available at 0.75° and 0.25° resolution respectively. Quantitative comparisons between the models are made at the ERA-Interim resolution of 0.75°. We also examine surface soil moisture and latent and sensible heat fluxes from the ERA-Interim 0600 forecast initialised at 0000 UTC (ERA-Interim/Land: Balsamo *et al.*, 2015) and the ERA5 0600 UTC reanalysis (ERA5L: Hersbach and Dee, 2016). The forecast product is used for ERA-Interim because the reanalysis product does not include surface fluxes. Temperature, sensible-heat flux and zonal wind component from the three models are also interpolated onto the flight track for comparison with *in situ* aircraft observations.

Soil moisture in the three models is initialised in a similar way. The model computes a "first guess" soil moisture and near-surface atmospheric state based on a short-term forecast. This model state is then analysed against observations. Differences between the observations and model state are reduced by uniformly adding or removing soil moisture from the near-surface soil layers. The ERA-Interim analysis uses observations of screen-level variables (2 m temperature and humidity: ECMWF, 2007). Soil moisture is added (removed) to increase (decrease) evapotranspiration and hence cool (warm) the model, to bring the near-surface atmospheric state closer to the observations. ERA5 and NCUM additionally assimilate Advanced SCATerometer (ASCAT) observations of soil moisture (de Rosnay *et al.,* 2011; George *et al.,* 2016) to constrain the soil moisture. The resulting soil moisture analysis is used as the initial soil moisture state.

2.4 | Synoptic and land surface conditions

Just prior to 30 June 2016, the synoptic conditions were dominated by active monsoon flow, with moist air from the Bay of Bengal (BoB) reaching parts of northwestern India. This resulted in rainfall on 28 June and to a lesser extent on 29 June. The easterly winds from the BoB persisted on the day of the flight (Figure 1a), but rainfall activity was restricted to central India, as a ridge started to develop at 500 hPa over northwest India. In the region of the flight, ERA-Interim 925 hPa winds depict a shear zone around 29°N, 73.7°E to 25°N, 77.2°E between easterly and westerly flows (Figure 2a) on the southwesterly edge of a warm air mass. Cooler air temperatures are evident towards the southwest and northeast and there is evidence of confluence on the shear zone, with easterlies to the east and westerlies to the west. During the flight, there were shallow cumulus clouds between 74.8°E and 76.8°E with the remainder of the track being predominately cloud free. According to the only high-resolution radiosonde data available in the region, by the end of the day (1730 hr/1200 UTC) the PBL had reached a height of approximately 2 km at Gwalior (26.2°N, 78.2°E).

The flight sampled the PBL above regions of contrasting land cover (Figure 2b) and rainfall history (Figure 2e). West of 76.4°E the vegetation was generally very sparse with some evidence of cropping and isolated trees covering a small percentage of the surface. Along the remainder of the flight path, a significant proportion of the land was made up of green fields. This is consistent with extensive irrigation in the relatively flat region east of 77°E, the Ganges valley. The terrain west of the irrigated region was characterized by gradual inclines with a couple of forested ridges (Figure 2b). Figure 2c,d show the two-dimensional structure of our proxies for surface wetness on or near the flight track. For clarity, we define three sections based on large-scale surface hydrological features. In the central section (74.5–77°E) the surface is predominately warm and dry while to the west (73.2–74.5°E) and east (77–79°E) the surface is cooler and wetter. Values of PR and LST are low in the western section due to antecedent rain (Figure 2e,f). There is no indication of rainfall in the 24 h

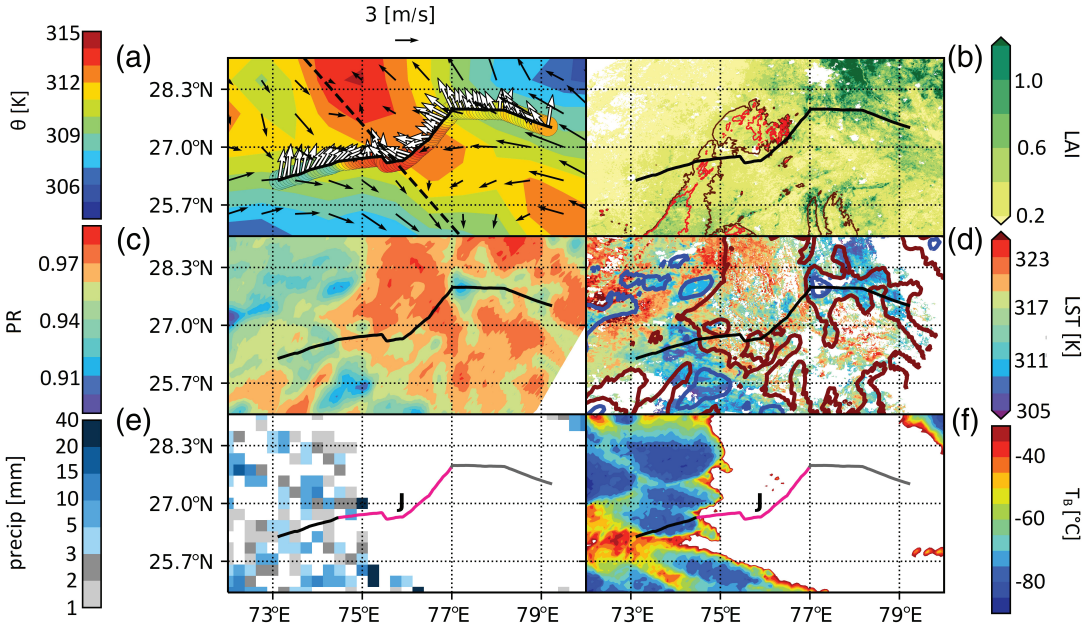

FIGURE 2 Low-level transect of INCOMPASS flight B968 on 30 June 2016 (solid line). (a) Potential temperature, θ (K), and wind vectors (m/s) along the flight track and plotted from ERA-Interim at 925 hPa and 0600 UTC (shading). The location of the shear zone is indicated by the straight dashed line. (b) Composite 8-day Leaf Area Index (LAI) in the region of the flight produced from combined Terra and Aqua MODIS data by NASA (Knyazikhin *et al.*, 1999) and selected surface elevation contours: 400 (m) (brown) and 500 (m) (red). (c) Polarization Ratio (PR) in the region of the flight derived from GPM polarized brightness temperatures at 10.7 GHz. (d) MODIS Land Surface Temperature, LST (K) (shading), from the Terra overpass on 30 June 2016 in the region of the flight and selected PR contours: 0.93 (blue solid line, outlining wetter surfaces) and 0.96 (dark red solid line, outlining drier surfaces). (e) 24 h accumulated precipitation (IMD-NCMRWF), precip. (mm), up to 0300 UTC (0830 hr) on 30 June 2016. (f) Minimum cloud-top brightness temperatures ($T_B < -30$ °C) measured by Meteosat-7 during the 24 h prior to the flight (up to 0500 UTC/1030 hr on 30 June 2016). In (e,f) the transect is separated by colour into the western (black), central (pink) and eastern (grey) sections defined in the text and the location of Jaipur (J) is included for reference. White areas in (b,c,d) denote missing data

prior to the flight in the central and eastern sections. In the eastern section, low values of PR and LST are due to active irrigation; surface and vegetation water content reduce PR, whilst high evapotranspiration suppresses LST. Climatologically the region of Rajasthan (west) is warmer than the state of Uttar Pradesh (east), and LSTs are 4 K cooler on average in the irrigated region (not shown) (Gallego-Elvira *et al.,* 2016).

3 | IMPACT OF SOIL MOISTURE ON THE PLANETARY BOUNDARY LAYER

3.1 | Observations

We now examine measurements of PBL and surface properties along the aircraft track. Figure 3a illustrates large-scale variation in potential temperature, θ. This is negatively correlated with specific humidity, q (Figure 3b). In the central section there is a 400 km warm and dry feature with cooler and moister sections to the east and west; in the west (east), the PBL is up to 5 (2.5) K cooler, and 4 (2) g/kg moister. The along-track wind component is positive (with the aircraft) in the west and predominately negative (against the aircraft) in the east, with a transition in the central section (Figure 3c). Turbulent heat flux, $<w'\theta'>$, fluctuates greatly along the flight path, though in general the values are low in the eastern and western sections and high in the central section (Figure 3d). Cooler PBL temperatures, higher PBL humidity and smaller magnitudes of $<w'\theta'>$ in the western and eastern sections coincide with generally lower values of PR and surface temperatures (Figure 3d,e). As discussed above, in the west these values are consistent with soil moisture from antecedent rain, whilst in the east, they are associated with irrigation. Overall, differences in surface wetness are clearly affecting the thermodynamic properties of the PBL in these three sections.

Within the wetter eastern and western sections there is also a clear correlation between surface properties and atmospheric variables at smaller scales. Zones of lower surface temperature of 20–60 km in extent around 73.8, 74.3, 77.2, 78 and 78.67°E (Figure 3e) coincide with locally lower values of PR, θ and $<w'\theta'>$, and locally higher values of q (Figure 3a,b,d). There is minimal vegetation in the western section, as indicated by LAI (Figure 3f) and confirmed by the flight logs made by on-board observers (not shown). This implies that local variations in PBL temperature and humidity are induced by soil moisture availability at the surface. The

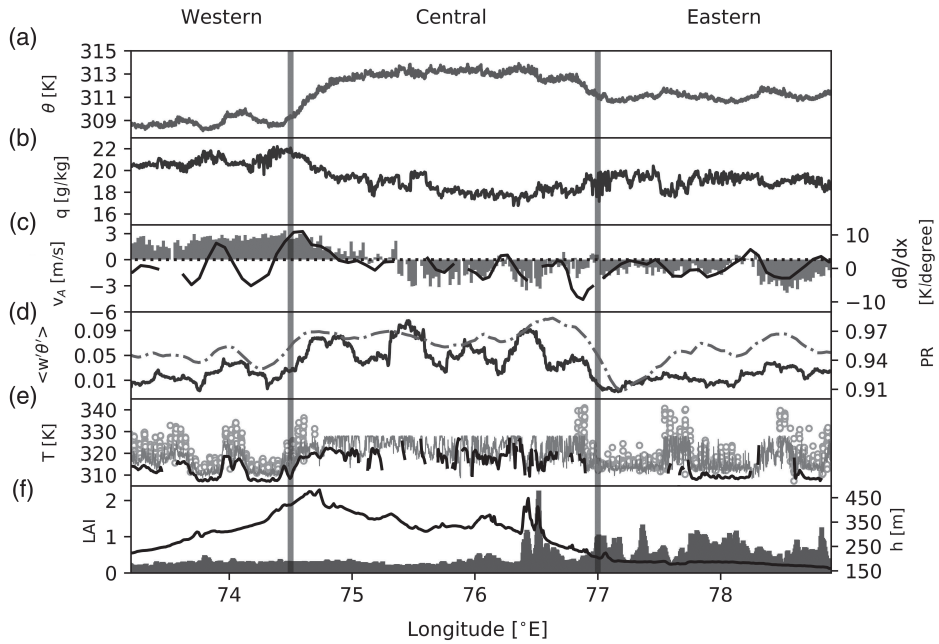

FIGURE 3 Aircraft data from the low-level transect and satellite data interpolated onto the flight track. (a) Potential temperature, θ (K). (b) Specific humidity, q (g/kg). (c) Along-track component of the wind, v_A (m/s) (shading) and along-track gradient in potential temperature for a length-scale of 60 km, $d\theta/dx$ (K degree^{-1}) (solid line). Values of $d\theta/dx$ and v_A are not shown when the aircraft is turning. (d) Vertical turbulent heat flux, $<w'\theta'>$ (solid line) and Polarization Ratio, PR, derived from GPM polarized brightness temperatures at 10.7 GHz (dash-dot). (e) Surface brightness temperature (K) measured by the Heimann radiometer (solid grey line), ARIES skin temperature (K) (circles) and MODIS Land Surface Temperature (K) (solid black line). ARIES data have been removed for regions affected by cloud. (f) Eight-day Leaf Area Index, LAI (shading) and surface elevation, h(m) (solid line)

driver of this variability in the eastern section may be a combination of soil moisture introduced by human activity and the resulting vegetation. Considering local wind anomalies, in the eastern section (and to a lesser extent, the central section), fluctuations in the along-track component are rather coherent with the along-track temperature gradient (Figure 3c). In the eastern section, the winds are broadly divergent above cool wet areas and convergent over the distinctly drier, warmer land surface features (Figure 3c,d). A relationship between small-scale wind anomalies and land surface features is not evident in the western section. However, the strongest along-track winds were recorded around 74.5°E, coinciding with the boundary between the rain-affected western section and dry central section.

In summary, the observed thermodynamic properties of the PBL are responding to surface heterogeneity on different spatial scales along the whole transect. The PBL is cooler and moister above wetter and/or more vegetated surfaces and there is evidence of divergent winds above some wet patches.

3.2 | Model comparison

3.2.1 | Low-level transect

We now compare observed variables along the flight track with the NCUM 30-hour forecast and the two reanalysis products. Figure 4 shows the comparison of PBL temperature (Figure 4a), sensible-heat flux (Figure 4b) and zonal component of the wind (Figure 4c). NCUM is too hot over the eastern section, consistent with excessive sensible-heat flux east of 77°E. In ERA-Interim sensible-heat flux falls off in the irrigated region, and contributes to cooler temperatures east of 77°E. Compared to ERA-Interim, ERA5 has slightly warmer temperatures in this section, corresponding to higher sensible-heat flux. Both ERA-Interim and NCUM underestimate the temperature gradient around 74.5°E, where rain had fallen the previous day to the west. ERA5 captures this transition better, though this is not consistent with variability in the along-track sensible-heat flux. The lower sensible-heat flux in ERA5 in the central section (relative to the western and eastern sections) presumably contributes to the model being too cold between 74.5 and 77°E. NCUM provides the most realistic description of PBL temperatures in the central section.

Both reanalyses and the forecast model capture the transition from westerlies in the west to easterlies in the east, though the location and strength of the shear zone differs (Figure 4c). This is linked to different temperature gradients. In the eastern section and in the far west, ERA5 gives the most realistic along-track description of the magnitudes of the winds. Both NCUM and ERA-Interim predict much stronger flow in the west.

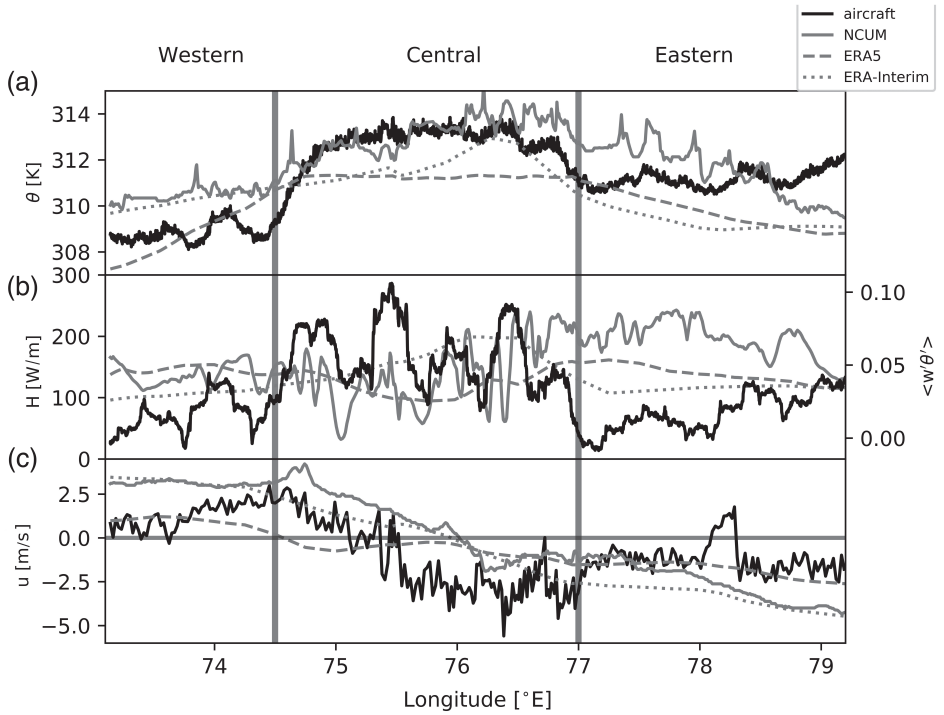

FIGURE 4 Aircraft data from the low-level transect (solid black line) and model data interpolated onto the flight track (NCUM – solid grey line, ERA5 – dashed line, ERA-Interim – dots). (a) Potential temperature, θ (K). (b) Sensible-heat flux, H (W m^{-2}) (models) and vertical turbulent heat flux, $<w'\theta'>$ (aircraft). (c) Zonal wind component, u (m/s)

In summary, when comparing with observations along the aircraft track, we see significant local errors in the model representation of thermodynamic changes over different surfaces, and no model is appreciably better than the others when considering the entire transect. This could be due to a number of reasons, for example, errors in the representation of vegetation and/or soil moisture, or inaccuracies in simulated precipitation driving erroneous spatial heterogeneity.

3.2.2 | Whole domain

We now assess the NCUM, ERA5 and ERA-Interim model outputs over a large domain during the flight (0600 UTC). At the surface, all models exhibit strong spatial variability in evaporative fraction (EF, Figure 5a,d,g). These patterns are largely controlled by soil moisture (not shown) and, in the absence of strong gradients in cloud cover, are associated with similar structures in sensible-heat flux during the morning. In the region of the flight track, spatial structures of wet/dry areas in the three models are broadly similar to observed PR and LST, our proxies for surface wetness (Figure 2c,d). Around the central section the surface is predominately dry, while wetter areas are indicated to the north and south of the western section. The very moist irrigated area around the eastern section is represented differently in the three models. ERA-Interim depicts wetter surfaces (EF > 0.8) around the whole of the eastern section, while ERA5 and NCUM place the wet area further to the east.

There is evidence of spatial correlations between the drier surfaces over the central section and higher PBL temperatures (Figure 5b,e,h). All three models depict a warm corridor of air orientated southeastward from the Indo-Pakistani border across the flight track. This feature extends from a hot air mass over Pakistan and separates cooler air masses in the east, from the BoB, and in the southwest, from the Arabian Sea. In NCUM, at 0600 UTC, the PBL temperatures associated with the warm air corridor are 2–3 K higher than in both ECMWF reanalyses, consistent with comparatively lower EF (and thus higher sensible-heat flux) at the surface (Figure 5a,b). In ERA5 PBL temperatures greater than 312 K are restricted to the northwest, where the EF at the surface is lower (EF < 0.4, Figure 5d,e). In ERA-Interim, southeast of the Indo-Pakistani border, PBL temperatures greater than 313 K are found over the drier surfaces (EF < 0.4, Figure 5g,h). In all three models the warm air corridor appears to be growing along drier zones to the southeast of the track. Overall it could be inferred that the surface fluxes are influencing the structure of the warm air corridor, since the PBL cannot heat up as quickly above areas of low sensible-heat flux (high EF). The warm air corridor is associated with an extension of the heat-low from the arid regions of the northwest southeastwards into the Indo-Gangetic plain, forming the main axis of the monsoon trough. Therefore these inter-model differences in PBL temperature are large enough to influence the structure of the monsoon trough (Figure 5c,f,i).

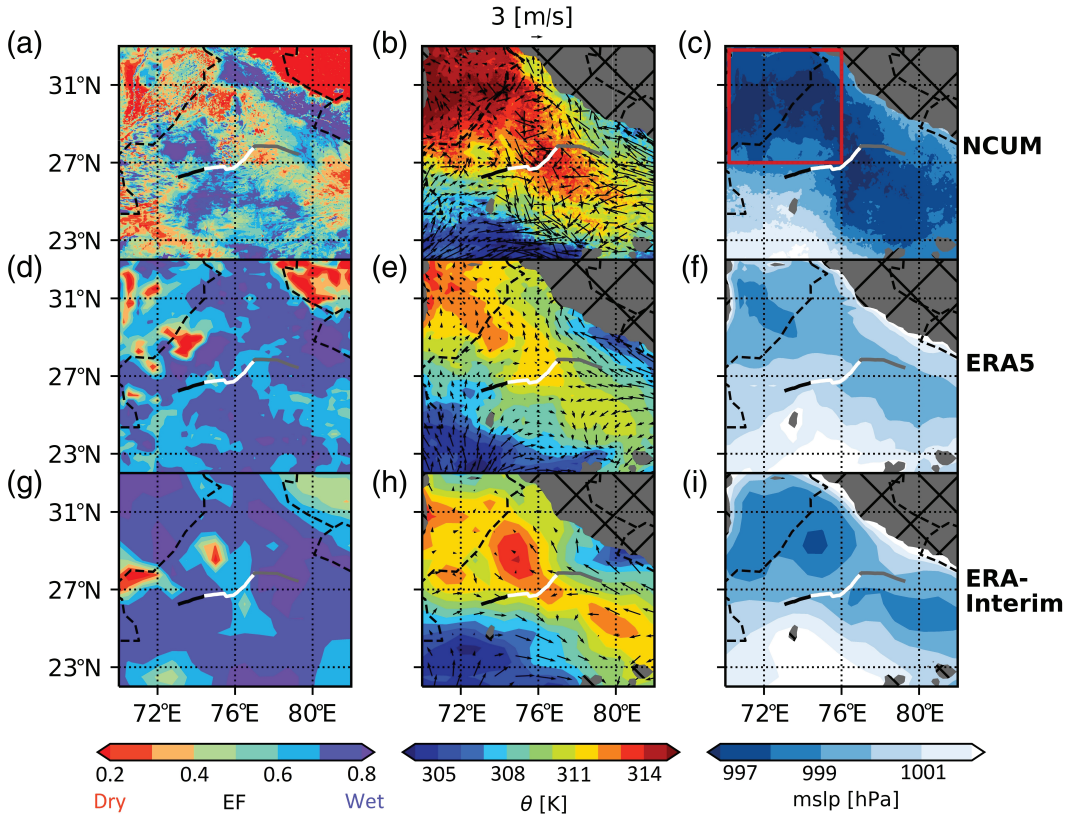

FIGURE 5 Low-level transect of INCOMPASS flight B968 on 30 June 2016 (solid line) and variables plotted from (a–c) the high-resolution NCUM simulation, (d–f) ERA5 and (g–i) ERA-Interim (shading). (a,d,g) Evaporative fraction, EF, of 6 h accumulated fluxes (0000–0600 UTC), (b,e,h) potential temperature, θ (K), and wind vectors (m/s) at 925 hPa and 0600 UTC, (c,f,i) mean-sea-level pressure, mslp (hPa). The transect is divided by shade into the western (black), central (white) and eastern (grey) sections defined in the text. The red box in (c) indicates the area used to generate the time series in Figure 7

To illustrate more clearly the impact of surface fluxes on the PBL, Figure 6 shows the differences between ERA-Interim and the higher-resolution models NCUM (Figure 6a,c,e,g) and ERA5 (Figure 6b,d,f,h). Here NCUM and ERA5 variables are presented at the ERA-Interim resolution of 0.75°. NCUM is around 2 K hotter than ERA-Interim across most of the domain (Figure 6a). These positive temperature biases are broadly coherent with reductions in EF exceeding 0.2 (Figure 6c). The domain average differences in temperature and EF are 1.1 K and −0.12 respectively. For ERA5 versus ERA-Interim, west of 77°E, areas of cooler/warmer PBL temperatures in ERA5 are correlated with areas of higher/lower EF (Figure 6b,d). The domain average differences in temperature and EF are −0.5 K and 0.04 respectively.

The inter-model differences in surface fluxes, and hence PBL temperature, influence the low-level winds. To illustrate this, divergence calculated using the difference wind fields is shown in Figure 6e,f. For clarity a few significant features are labelled A–I. In the NCUM/ERA-Interim difference wind field, on the whole there is more convergence in regions where EF is lower in NCUM. For example, there is convergent flow around A, to the northwest (B) and southwest (C) of this patch and further south (D). There is also divergent flow around E where NCUM is cooler and wetter. In the ERA5/ERA-Interim difference wind field, divergent flow is present around F and G where ERA5 is cooler and wetter, while the difference wind field converges around H and I where ERA5 is warmer and drier. Overall, in regions where there is clear correlation between differences in EF and PBL temperature, the low-level winds are also affected.

As mentioned above, the inter-model difference in surface fluxes also influences the monsoon trough. Figure 6g reveals that mean-sea-level pressure (mslp) in NCUM is ∼2 hPa lower than ERA-Interim when averaged across the whole domain. To investigate the origins of this bias, we examine a 2-day time series of mslp from the start of the NCUM simulation over the northwestern quadrant (shown in Figure 5c), where the lowest pressures are found in all three models. Figure 7a shows that, after 1 h, NCUM has a low-pressure bias of 0.7 hPa which increases to 1.7 hPa by sunset on 29 June. This bias decreases slightly overnight, then grows rapidly after sunrise on 30 June, reaching 3.4 hPa at sunset. The timing of these changes is consistent with the evolution of inter-model differences in simulated temperature (not shown) and sensible-heat flux (shown for NCUM and ERA5

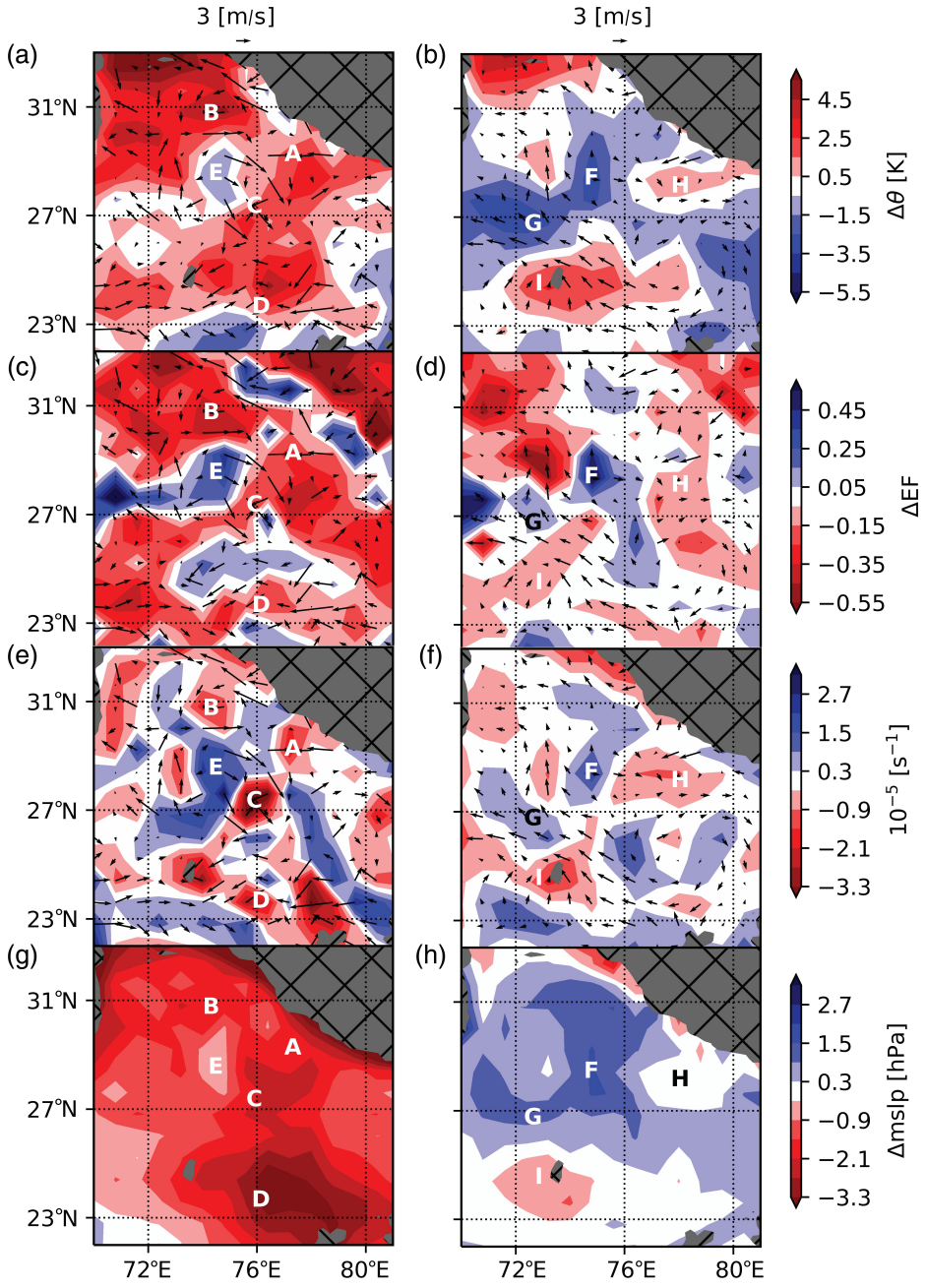

FIGURE 6 Model comparison between: (a,c,e,g) NCUM and ERA-Interim; (b,d,f,h) ERA5 and ERA-Interim. (a,b) Difference in potential temperature, $\Delta\theta$ (K). (c,d) Difference in evaporative fraction, ΔEF. (e,f) Difference in divergence (s^{-1}). (g,h) Difference in mean-sea-level pressure, Δmslp (hPa). In (a–f), differences in the wind field are shown by the arrows (m/s). Labels A–I identify features discussed in the text

in Figure 7b). Peak sensible-heat flux in NCUM has increased by 34 W m^{-2} from 29 June to 30 June, whilst it is similar in ERA5 between the two days. Overall, this implies that higher sensible-heat fluxes in NCUM are inducing a significant (~3.5 hPa) inter-model difference in surface pressure after just 38 h.

In summary, for this case-study we show that model-dependent soil moisture initialisation affects simulated PBL temperature, mslp and wind fields through soil moisture–atmosphere coupling. We find evidence indicating that inter-model surface flux differences are large enough to impact the monsoon trough structure and intensity. At finer spatial scales, we find that wet/dry patches generate local divergent/convergent flows in some locations.

4 | IMPACT OF SOIL MOISTURE GRADIENTS ON CONVECTION

Having analysed soil moisture impacts on PBL thermodynamics, we now consider the evolution of convective cloud in the region of the flight from satellite observations. Figure 8 displays MODIS true colour satellite

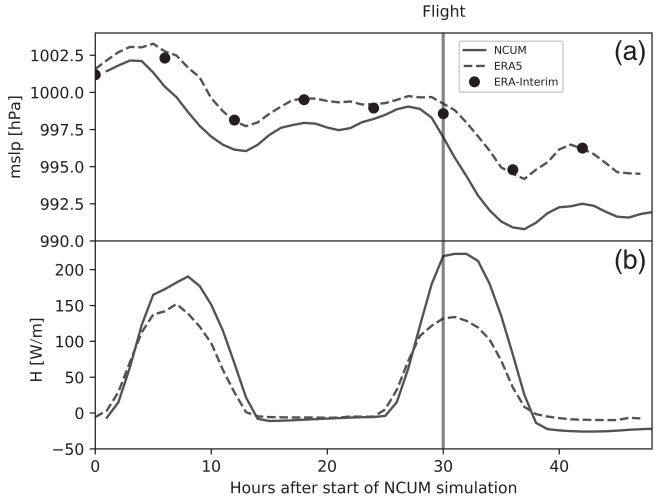

FIGURE 7 Two-day time series of modelled variables averaged over 27–33°N, 70–76°E. (a) Mean-sea-level pressure, mslp (hPa). (b) Sensible-heat flux, H (W m^{-2}). Solid (dashed) lines denote NCUM (ERA5). Circles in (a) represent ERA-Interim

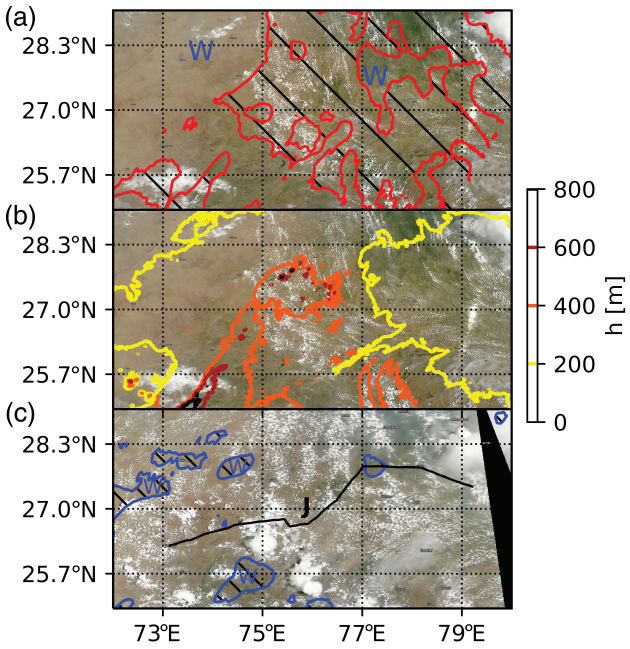

FIGURE 8 MODIS true colour satellite imagery from the (a,b) Terra (0500 UTC/1030 hr) and (c) Aqua (0800 UTC/1330 hr) overpasses in the region of the flight. (a) Polarization Ratio contour 0.96 (red solid line with hatching) outlines drier surfaces. (b) Surface elevation contours, *h (m)*. (c) Polarization Ratio contour 0.93 (blue solid line with hatching) outlines wetter surfaces. The low-level transect of INCOMPASS flight B968 on 30 June 2016 and the location of Jaipur (J) are included in (c) for reference. "W" and "D" labels indicate wetter and drier areas respectively

imagery from the Terra and Aqua overpasses on 30 June 2016. These provide snapshots of cloud cover approximately half an hour before (Terra) and 1 h after (Aqua) the flight.

At the time of the Terra overpass (0500 UTC/1030 hr) there is extensive shallow cumulus cloud cover over drier areas and there are predominately cloud-free skies over wetter areas (Figure 8a). Cloudy areas along the flight track, as detected by radiometers on the aircraft, are also correlated with higher surface and PBL temperatures (not shown). The shallow clouds are not exclusive to higher elevations (Figure 8b), suggesting that topography is not the dominant forcing of the cloud field. Suppression of shallow cloud formation appears to persist for the wettest patches, at least until the time of the Aqua overpass (0800 UTC/1330 hr, Figure 8c).

By the early afternoon, deep clouds have formed in several locations in the region of the flight (Figure 9a). Half-hourly M7 data were used to monitor the development of convective storms that initiated close to the flight path. The locations where cloud-top temperatures first dropped below −30 °C for 17 cold cloud areas are marked with symbols in Figure 9b,c. The seven locations marked by a triangle either follow a steep ridge or coincide with the cool air flow from the Arabian Sea intersecting topography (Figure 9a). This suggests a strong influence of orography on triggering deep convection in these cases. The link between topographical features and the remaining initiations is less obvious (Figure 9a,b). The eight locations marked by a star form a band of convective initiations broadly parallel to, and on the dry side of, a wet–dry boundary (Figure 9c). This band is in the region of the confluence captured by the aircraft wind observations and depicted in the models in the surrounding area (Figure 9a and 5b,e,h). The remaining locations, marked by a circle, lie broadly in the shear zone where, we assume, the cool flow from the Arabian Sea meets the hot air mass over Pakistan. There are no aircraft observations in this area to confirm exactly where the two air masses meet; however, these storms initiated over locally drier soils (Figure 9c).

In summary, on this day we observe mid-morning shallow cloud suppression over wetter soils. Deep convective storms developed in the early afternoon along a steep ridge, in locations where background air flow intersects topography and on the dry side of wet–dry boundaries in areas of large-scale confluence. The latter cases suggest a role for mesoscale soil moisture structures in organizing the initiation of deep convection, although strong conclusions cannot be drawn from a single case-study.

5 | DISCUSSION

This work presents a case-study of land–atmosphere interactions in northern India. Flight B968 on 30 June 2016 from the INCOMPASS field campaign sampled PBL variability on a range of spatial scales that we attribute to soil moisture availability at the surface. Aircraft observations and satellite data presented here clearly demonstrate the changes in thermodynamic properties of the PBL induced by recently wetted surfaces and irrigation. The PBL was observed to be up to 5 and 2.5 K warmer, 4 and 2 g/kg drier in the central

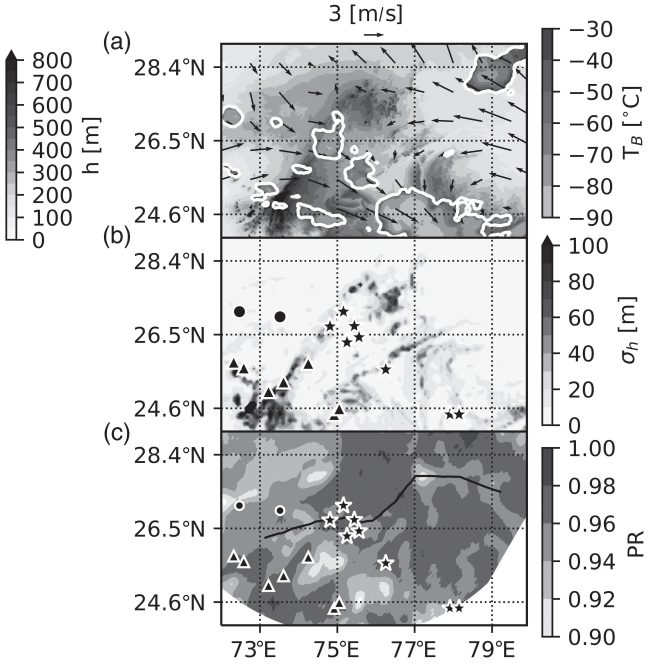

FIGURE 9 Convective cloud in the region of the flight. (a) Surface elevation, h (m) (background shading), cloud-top brightness temperatures ($T_B < -30$ °C) measured by Meteosat-7 at 0930 UTC (1500 hr) highlighting deep clouds (outlined in white) and wind vectors (m/s) plotted from ERA-Interim indicating large-scale flow. (b) Standard deviation in topography over a 5×5 pixel box, σ_h (m) (background shading). (c) Polarization ratio (PR) in the region of the flight derived from GPM polarized brightness temperatures at 10.7 GHz (background shading). The low-level transect of INCOMPASS flight B968 on 30 June 2016 (solid black line) is included in (c) for reference. Star, triangle and circle markers (discussed in the text) in (b,c) denote the locations where the cloud-top brightness temperatures first drop below −30 °C for 17 cold cloud areas that initiated near the flight path

section, compared to the rain-fed western and irrigated eastern sections respectively. These are the first such *in situ* observations of PBL responses to irrigation and antecedent rain over India. The response to antecedent rain is larger than observed in previous studies in the West African monsoon region (Taylor *et al.,* 2007; Dixon *et al.,* 2013). Specifically, the amplitude of temperature variation observed here was up to 2 K stronger than reported in Taylor *et al.* (2007). The response to irrigation is comparable to a 2–3 K difference in PBL temperature reported by Mahrt *et al.* (1994) over irrigation in California. The West African and American studies also report evidence of mesoscale circulations driven by soil moisture heterogeneity. Consistent with this, we find observational evidence of divergent (convergent) wind flow above wetter (drier) surfaces. For India there is likely to be additional complexity which has not been captured by the aircraft observations analysed in the current work. Analysis of other flights in the INCOMPASS campaign may provide additional information on these interactions.

We observe an apparent impact of irrigation on the atmosphere which is comparable to antecedent rain. This is an important result as irrigation across northern India is extensive (FAO, 2014). We would expect irrigation-induced daytime gradients in the PBL to persist from day to day, and indeed there is evidence for this from preliminary analysis of other INCOMPASS flights (not shown). By contrast, soil moisture patterns created by antecedent rainfall are transient. The impact of irrigation on temperature and wind patterns implies that historical changes in irrigation are likely to have influenced mesoscale processes within the Indian summer monsoon and, perhaps more importantly, future changes are likely to do the same. Indeed, the size of irrigated area is set to increase, at least in the short term (Dhawan, 2017). The impact of irrigation needs to be taken into account when modelling and forecasting the Indian summer monsoon. Similar conclusions have been drawn from modelling studies (e.g. Douglas *et al.,* 2009). Without detailed information on the spatial distribution and type of irrigation, weather forecast models may not be able to predict key PBL processes, including the development of convective cloud (e.g. Lawston *et al.,* 2015). Climate models will additionally require information on the temporal variation of irrigation usage in order to reproduce historical trends and predict future changes in the Indian summer monsoon.

It is interesting to compare our spatial observations of PBL temperature and humidity over wet and dry regions in northern India to an analysis of temporal variations in atmospheric conditions during active and break spells of the monsoon in southeast India by Monhan and Rao (2012). Based on radiosonde data obtained during the 2006–2009 monsoon seasons, they estimate a difference in mean temperature and humidity between wet and dry spells of 1–2 K and 0.5–2 g/kg in the lower troposphere. Such intraseasonal land–atmosphere feedbacks are consistent with new observations from the Indian surface flux network set up as part of INCOMPASS (Bhat *et al.,* 2019). These confirm the existence of substantial intraseasonal fluctuations in evaporative fraction at drier sites. In the current work, the difference in mean PBL temperature and humidity over wet (eastern and western) and dry (central) sections was found to be 3 K and 1.3 g/kg. It would be worthwhile to investigate further by analysing more observations, in particular existing radiosonde data from northern India, and hence study the role of the land surface in influencing PBL fluctuations on intraseasonal time-scales.

We have analysed outputs from three models, each providing a different depiction of 30 June 2016. All models capture the moist irrigated region to the east of the flight track to some degree. Irrigation is not explicitly considered in the models, although the impact of increased soil moisture may be captured implicitly through assimilation of screen-level variables (e.g. ECMWF, 2007) to nudge soil moisture at initialisation. The western extent of the irrigated region differs between the

models, presumably due to differences in soil moisture initialisation, and we find ERA-Interim to be in best agreement with satellite observations. In fact, the top-level soil moisture in this model is highest over the irrigated region, consistent with recent work by Tuinenburg and de Vries (2017) that highlighted a relationship between irrigation and soil moisture increments in the ERA-Interim data assimilation system.

The detailed structure of the monsoon trough in each model is significantly modified by the land surface, and none of the models have accurately reproduced the observations. Evidence presented here indicates that surface flux uncertainties in the 38-hour forecast lead to a significant bias of 3.4 hPa (relative to the reanalysis) in the monsoon trough. Such biases will impact large-scale shear and confluence associated with the monsoon trough in the models and have implications for the modelling of the larger-scale circulation and rainfall prediction. It would be informative to perform soil moisture sensitivity tests to see whether different soil moisture initialisations change the large-scale temperature and pressure structure for this well-observed day. For NCUM it would also be important to look at systematic biases in forecasts of the monsoon trough, to discern whether this particular case is (a) typical, and (b) associated with too much surface insolation and/or too dry a surface at initialisation.

The observed organisation of deep convection by soil moisture in this work is consistent with the findings of previous work. Modelling studies (e.g. Osuri *et al.,* 2017) have demonstrated that land surface features can interact with synoptic-scale circulations and hence play a significant role in mesoscale convection. Eight of the cold cloud areas tracked in this work were found to initiate on the dry side of a wet–dry soil moisture boundary that coincided with an area of large-scale shear and confluence associated with the monsoon trough. This apparent preference of convective storms to initiate over locally drier soils has been reported previously for the Sahel (Taylor *et al.,* 2011). It is our intention to perform a similar statistical analysis to Taylor *et al.* (2011) for northern India to determine the impact of soil moisture on convective initiation in the region.

On the topic of shallow clouds, suppression of cloud formation over wetter regions has been observed previously, for example over irrigation in China (Sato *et al.,* 2007; Kawase *et al.,* 2008), with contrary findings in Saudi Arabia (Garcia-Carreras *et al.,* 2017). Modelling studies (e.g. Ek and Holtslag, 2004; Haiden, 2007; Huang and Margulis, 2011; Chlond *et al.,* 2014; Bhowmick and Parker, 2018) suggest that the influence of soil moisture on shallow cloud development depends heavily on thermal stability conditions and vertically integrated atmospheric moisture content. Unfortunately, we do not have the necessary vertical information to assess the atmospheric stability conditions on the day of the flight. However, our observations are consistent with a negative soil moisture–cloud cover feedback, whereby cloud formation is enhanced over dry soils with high sensible-heat flux due to increased heating and PBL growth (Pielke, 2001; Findell and Eltahir, 2003; Ek and Holtslag, 2004).

Our results have indicated that soil moisture gradients may play a significant role in the development of deep convection during the early phases of the Indian summer monsoon, by influencing both large-scale shear and the location of convective initiation along lines of confluence. Characterizing this feedback could be an important step towards improving the forecasting of monsoon rain by, for example, informing development of new parametrization schemes.

6 | CONCLUSIONS

1. The airborne observations show clear evidence of land surface control on the atmosphere, on scales from 20 to 200 km. The amplitude of PBL temperature fluctuations in response to the land surface is larger than the observed responses in the Sahel and is caused both by antecedent rainfall and irrigation.
2. Patterns of shallow cloud correspond well to regions of low soil moisture, indicating an important role of land surface state in the development of shallow convection. Deep convection developed either in association with topography or on the dry side of soil moisture gradients.
3. The tested models agree on large-scale patterns of shear and confluence crossing the flight track and extending along the monsoon trough. These patterns are consistent with the larger-scale forcing for the regional circulation.
4. The models all show a strong thermodynamic response to the land surface which significantly modifies the thermal and pressure structure of the shear zone. The differing land-surface state between the models accounts for inter-model differences in the structure of the atmospheric features.
5. The differences between the thermodynamics and winds in the models are significant, and all differ from the observations. This will feed back on subsequent rainfall which will cause errors to persist and amplify.

ACKNOWLEDGEMENTS

We would like to warmly thank all those involved in the India deployment of the FAAM aircraft. This study was funded by the joint NERC/MoES INCOMPASS project (NERC grant references NE/L013819/1, NE/L01386X/1, NE/L013843/1 and NE/P003117/1). Brooke was supported by the Met Office Public Weather Service funding. Harlow was funded through the Met Office for this project. Parker has been supported by a Royal Society Wolfson Research Merit Award (2014-2018).

Böing is partially funded through the NERC/Met Office joint programme GENESIS (NE/L013840/1).

ORCID

Emma J. Barton https://orcid.org/0000-0001-5945-9244
Christopher M. Taylor https://orcid.org/0000-0002-0120-3198
Douglas J. Parker https://orcid.org/0000-0003-2335-8198
Andrew G. Turner https://orcid.org/0000-0002-0642-6876
Steven J. Böing https://orcid.org/0000-0003-3794-2563
Kieran Hunt https://orcid.org/0000-0003-1480-3755
A. Jayakumar https://orcid.org/0000-0002-1497-6042

REFERENCES

Asharaf, S., Dobler, A. and Ahrens, B. (2012) Soil moisture–precipitation feedback processes in the Indian summer monsoon season. *Journal of Hydrometeorology*, 13, 1461–1474.

Balsamo, G., Albergel, C., Beljaars, A., Boussetta, S., Brun, E., Cloke, H., Dee, D., Dutra, E., Muñoz-Sabater, J., Pappenberger, F., de Rosnay, P., Stockdale, T. and Vitart, F. (2009) ERA-Interim/Land: a global land surface reanalysis data set. *Hydrology and Earth System Sciences*, 19, 389–407. https://doi.org/10.5194/hess-19-389-2015.

Bhat, G.S., Morrison, R., Taylor, C.M., Bhattacharya, B.K., Paleri, S., Desai, D., Evans, J.G., Pattnaik, S., Sekhar, M., Nigam, R., Sattar, A., Angadi, S.S., Kacha, D., Patidar, A., Tripathi, S.N., Krishnan, M. and Sisodiya, A. (2019) Spatial and temporal variability in energy and water vapour fluxes across the India, (in press).

Bhowmick, M. and Parker, D.J. (2018) Analytical solution to a thermodynamic model for the sensitivity of afternoon deep convective initiation to the surface Bowen ratio. *Quarterly Journal of the Royal Meteorological Society*, 144(716), 2216–2229. https://doi.org/10.1002/qj.3340.

Bollasina, M.A. (2014) Probing the monsoon pulse. *Nature Climate Change*, 4, 422–423. https://doi.org/10.1038/nclimate2243.

Boutle, I.A., Eyre, J.E.J. and Lock, A.P. (2014) Seamless stratocumulus simulation across the turbulent gray zone. *Monthly Weather Review*, 142(4), 1655–1668. https://doi.org/10.1175/MWR-D-13-00229.1.

Chlond, A., Bohringer, O., Auerswald, T. and Muller, F. (2014) The effect of soil moisture and atmospheric conditions on the development of shallow cumulus convection: a coupled large-eddy simulation land surface model study. *Meteorologische Zeitschrift*, 23, 491–510.

Dee, D.P., Uppala, S.M., Simmons, A.J., Berrisford, P., Poli, P., Kobayashi, S., Andrae, U., Balmaseda, M.A., Balsamo, G., Bauer, P., Bechtold, P., Beljaars, A.C.M., van de Berg, L., Bidlot, J., Bormann, N., Delsol, C., Dragani, R., Fuentes, M., Geer, A.J., Haimberger, L., Healy, S.B., Hersbach, H., Hólm, E.V., Isaksen, L., Kållberg, P., Köhler, M., Matricardi, M., McNally, A.P., Monge-Sanz, B.M., Morcrette, J.J., Park, B.K., Peubey, C., de Rosnay, P., Tavolato, C., Thépaut, J.-N. and Vitart, F. (2011) The ERA-Interim reanalysis: configuration and performance of the data assimilation system. *Quarterly Journal of the Royal Meteorological Society*, 137(656), 553–597. https://doi.org/10.1002/qj.828.

Dhawan, V. (2017) Water and Agriculture in India - Background Paper for the South Asia Expert Panel during the Global Forum for Food and Agriculture. New Delhi, India: The Energy and Resources Institute (TERI) Available at: https://www.oav.de/fileadmin/user_upload/5_Publikationen/5_Studien/170118_Study_Water_Agriculture_India.pdf. [Accessed September 2018].

Dixon, N.S., Parker, D.J., Taylor, C.M., Garcia-Carreras, L., Harris, P.P., Marsham, J.H., Polcher, J.a. and Woolley, A. (2013) The effect of background wind on mesoscale circulations above variable soil moisture in the Sahel. *Quarterly Journal of the Royal Meteorological Society*, 139(673), 1009–1024. https://doi.org/10.1002/qj.2012.

Douglas, E.M., Beltran-Przekurat, A., Niyogi, D., Pielke, R.A., Sr. and Vorosmarty, C.J. (2009) The impact of agricultural intensification and irrigation on land–atmosphere interactions and Indian monsoon precipitation – a mesoscale modeling perspective. *Global and Planetary Change*, 67, 117–128.

ECMWF. (2007) *IFS documentation Cy31r1, Part II: European Centre for mid range weather forecasts*. Technical Report. Reading, UK: ECMWF. Available at: http://www.ecmwf.int/sites/default/files/elibrary/2007/9219-part-ii-data-assimilation.pdf. [Accessed February 2019].

Ek, M.B. and Holtslag, A.A.M. (2004) Influence of soil moisture on boundary layer cloud development. *Journal of Hydrometeorology*, 5(1), 86–99. https://doi.org/10.1175/1525-7541(2004)005<0086:IOSMOB>2.0.CO;2.

FAO. (2014). *Food and Agricultrual Organisation of the United States. Area equipped for irrigation*. Prepared by AQUASTAT, FAO's global water information system: Food and Agriculture Organization of the United Nations. Available at: http://www.fao.org/nr/water/aquastat/infographics/Irrigation_eng.pdf. [Accessed March 2017].

Ferguson, C.R., Wood, E.F. and Vinukollu, R.K. (2012) A global intercomparison of modeled and observed land–atmosphere coupling. *Journal of Hydrometeorology*, 13(3), 749–784. https://doi.org/10.1175/JHM-D-11-0119.1.

Findell, K.L. and Eltahir, E.A.B. (2003) Atmospheric controls on soil moisture–boundary layer interactions. Part I: Framework development. *Journal of Hydrometeorology*, 4(3), 552–569. https://doi.org/10.1175/1525-7541(2003)004<0552:ACOSML>2.0.CO;2.

Findell, K.L., Gentine, P., Lintner, B.R. and Kerr, C. (2011) Probability of afternoon precipitation in eastern United States and Mexico enhanced by high evaporation. *Nature Geoscience*, 4(7), 434–439.

Gaertner, M.A., Domínguez, M. and Garvert, M. (2010) A modelling case-study of soil moisture–atmosphere coupling. *Quarterly Journal of the Royal Meteorological Society*, 136(S1), 483–495. https://doi.org/10.1002/qj.541.

Gallego-Elvira, B., Taylor, C.M., Harris, P.P., Ghent, D., Veal, K.L. and Folwell, S.S. (2016) Global observational diagnosis of soil moisture control on the land surface energy balance. *Geophysical Research Letters*, 43(6), 2623–2631. https://doi.org/10.1002/2016GL068178.

Gantner, L. and Kalthoff, N. (2010) Sensitivity of a modelled life cycle of a mesoscale convective system to soil conditions over West Africa. *Quarterly Journal of the Royal Meteorological Society*, 136(S1), 471–482. https://doi.org/10.1002/qj.425.

Garcia-Carreras, L., Marsham, J.H. and Spracklen, D.V. (2017) Observations of increased cloud cover over irrigated agriculture in an arid environment. *Journal of Hydrometeorology*, 18(8), 2161–2172. https://doi.org/10.1175/JHM-D-16-0208.1.

Garcia-Carreras, L., Parker, D.J. and Marsham, J.H. (2010) What is the mechanism for the modification of convective cloud distributions by land surface-induced flows? *Journal of the Atmospheric Sciences*, 68(3), 619–634. https://doi.org/10.1175/2010JAS3604.1.

George, J.P., Indira Rani, S., Jayakumar, A., Mohandas, S., Mallick, S., Lodh, A., Rakhi, R., Sreevathsa, M.N.R. and Rajagopal, E.N. (2016) *NCUM data assimilation system*. National Centre for Medium Range Weather Forecasting. Available at: http://www.ncmrwf.gov.in/NCUM-Data%20Assimilation.pdf. [Accessed September 2018].

Goel, M. and Srivastava, H.N. (1990) Monsoon trough boundary layer experiment (MONTBLEX). *Bulletin of the American Meteorological Society*, 71, 1594–1600.

GPM. (2014) *GPM GMI Level 1C common calibrated brightness temperatures collocated*. Available at: http://disc.gsfc.nasa.gov/datacollection/GPM_1CGPMGMI_V03.html. [Accessed February 2017].

Haiden, T. (2007) An analytical study of cumulus onset. *Quarterly Journal of the Royal Meteorological Society*, 123(543), 1945–1960. https://doi.org/10.1002/qj.49712354309.

Hersbach, H. and Dee, D. (2016) *ERA5 reanalysis is in production*. *ECMWF Newsletter*, 7, 147 Available at: https://www.ecmwf.int/en/elibrary/16299-newsletter-no-147-spring-2016.

Huang, H.-Y. and Margulis, S.A. (2011) Investigating the impact of soil moisture and atmospheric stability on cloud development and distribution using a coupled large-eddy simulation and land surface model. *Journal of Hydrometeorology*, 12(5), 787–804. https://doi.org/10.1175/2011JHM1315.1.

Jain, S. and Kumar, V. (2012) Trend analysis of rainfall and temperature data for India. *Current Science*, 102(1), 37–42.

Jayakumar, A., Rajagopal, E.N., Boutle, I.A., George, J.P., Mohandas, S., Webster, S. and Aditi, S. (2017) An operational fog prediction system for Delhi using the 330 m Unified Model. *Atmospheric Science Letters*, 19(1), e796. https://doi.org/10.1002/asl.796.

Joseph, P.V. and Sijikumar, S. (2004) Intraseasonal variability of the low-level jet stream of the Asian summer monsoon. *Journal of Climate*, 17, 1449–1458.

Kar, S.C., Mali, P. and Routray, A. (2014) Impact of land surface processes on the South Asian monsoon simulations using WRF modeling system. *Pure and Applied Geophysics*, 171, 2461–2484.

Kawase, H., Yoshikane, T., Hara, M., Kimura, F., Sato, T. and Ohsawa, S. (2008) Impact of extensive irrigation on the formation of cumulus clouds. *Geophysical Research Letters*, 35, L01806. https://doi.org/10.1029/2007GL032435.

Knyazikhin, Y., Glassy, J., Privette, J.L., Tian, Y., Lotsch, A., Zhang, Y., Wang, Y., Morisette, J.T., Votava, P., Myneni, R.B., Nemani, R.R. and Running, S.W. (1999) MODIS Leaf Area Index (LAI) and Fraction of Photosynthetically Active Radiation Absorbed by Vegetation (FPAR) Product (MOD15) Algorithm Theoretical Basis Document. Technical Report. NASA. Available at: https://modis.gsfc.nasa.gov/data/atbd/atbd_mod15.pdf [Accessed March 2017].

Koster, R.D., Dirmeyer, P.A., Guo, Z.C., Bonan, G., Chan, E., Cox, P., Gordon, C.T., Kanae, S., Kowalczyk, E., Lawrence, D., Liu, P., Lu, C.-H., Malyshev, S., McAvaney, B., Mitchell, K., Mocko, D., Oki, T., Oleson, K., Pitman, A., Sud, Y.C., Taylor, C.M., Verseghy, D., Vasic, R., Xue, Y.K. and Yamada, T. (2004) Regions of strong coupling between soil moisture and precipitation. *Science*, 305, 1138–1140.

Lawston, P.M., Santanello, J.A., Zaitchik, B.F. and Rodell, M. (2015) Impact of irrigation methods on land surface model spinup and initialization of WRF forecasts. *Journal of Hydrometeorology*, 16(3), 1135–1154. https://doi.org/10.1175/JHM-D-14-0203.1.

Lohou, F., Kergoat, L., Guichard, F., Boone, A., Cappelaere, B., Cohard, J.M., Demarty, J., Galle, S., Grippa, M., Peugeot, C., Ramier, D., Taylor, C.M.a. and Timouk, F. (2014) Surface response to rain events throughout the West African monsoon. *Atmospheric Chemistry and Physics*, 14(8), 3883–3898. https://doi.org/10.5194/acp-14-3883-2014.

Mahrt, L., Sun, J., Vickers, D., Macpherson, J.I., Pederson, J.R. and Desjardins, R.L. (1994) Observations of fluxes and inland breezes over a heterogeneous surface. *Journal of the Atmospheric Sciences*, 51(17), 2484–2499. https://doi.org/10.1175/1520-0469(1994)051<2484:OOFAIB>2.0.CO;2.

Mitra, A.K., Momin, I.M., Rajagopal, E.N., Basu, S., Rajeevan, M.N. and Krishnamurti, T.N. (2013) Gridded daily Indian monsoon rainfall for 14 seasons: merged TRMM and IMD gauge analyzed values. *Journal of Earth System Science*, 122(5), 1173–1182. https://doi.org/10.1007/s12040-013-0338-3.

Monhan, T.S. and Rao, T.N. (2012) Variability of the thermal structure of the atmosphere during wet and dry spells over southeast India. *Quarterly Journal of the Royal Meteorological Society*, 138, 1839–1851.

Myneni, R., Knyazikhin, Y. and Park, T. (2015) *MCD15A2H MODIS/Terra+Aqua Leaf Area Index/FPAR 8-Day L4 Global 500m SIN Grid V006 [Data Set]*.

Niyogi, D., Chang, H.-I., Chen, F., Gu, L., Kumar, A., Menon, S. and Pielke, R.A., Sr. (2007) Potential impacts of aerosol–land–atmosphere interactions on the India monsoonal rainfall characteristics. *Natural Hazards*, 42, 345–359.

Osuri, K.K., Nadimpalli, R., Mohanty, U.C., Chen, F., Rajeevan, M. and Niyogi, D. (2017) Improved prediction of severe thunderstorms over the Indian monsoon region using high-resolution soil moisture and temperature initialization. *Scientific Reports*, 7, 41377. https://doi.org/10.1038/srep41377.

Parker, D.J., Willetts, P., Birch, C., Turner, A.G., Marsham, J.H., Taylor, C.M., Kolusu, S.a. and Martin, G.M. (2016) The interaction of moist convection and mid-level dry air in the advance of the onset of the Indian monsoon. *Quarterly Journal of the Royal Meteorological Society*, 142, 2256–2272.

Paul, S., Ghosh, S., Oglesby, R., Pathak, A., Chandrasekharan, A. and Ramsankaran, R. (2016) Weakening of Indian summer monsoon rainfall due to changes in land use land cover. *Scientific Reports*, 6, 32177. https://doi.org/10.1038/srep32177.

Pielke, R.A., Sr. (2001) Influence of the spatial distribution of vegetation and soils on the prediction of cumulus convective rainfall. *Reviews of Geophysics*, 39(2), 151–177. https://doi.org/10.1029/1999RG000072.

Rakhi, R., Jayakumar, A., Sreevathsa, M.N.R. and Rajagopal, E. (2016) *Implementation and up-gradation of NCUM in Bhaskara HPC*. National Centre for Medium Range Weather Forecasting Ministry of Earth Sciences, Government of India A-50, Sector-62, NOIDA-201309, INDIA. Report NMRF/TR/03/2016. [Accessed September 2018].

Rochetin, N., Couvreux, F. and Guichard, F. (2017) Morphology of breeze circulations induced by surface flux heterogeneities and their impact on convection initiation. *Quarterly Journal of the Royal Meteorological Society*, 143(702), 463–478. https://doi.org/10.1002/qj.2935.

de Rosnay, P., Chiara, G.D. and Mallas, I. (2011) *Use of ASCAT soil moisture: revised bias correction and test of improved ASCAT product in IFS cycle*. Reading, UK: ECMWF.

Sandeep, A., Rao, T.N., Ramkiran, C.N. and Rao, S.V.B. (2014) Differences in atmospheric boundary-layer characteristics between wet and dry episodes of the Indian summer monsoon. *Boundary-Layer Meteorology*, 153, 217–236.

Sato, T., Kimura, F. and Hasegawa, A.S. (2007) Vegetation and topographic control of cloud activity over arid/semiarid Asia. *Journal of Geophysical Research*, 112, D24109. https://doi.org/10.1029/2006JD008129.

Sperber, K.R., Annamalai, H., Kang, I.S., Kitoh, A., Moise, A., Turner, A., Wang, B. and Zhou, T. (2013) The Asian summer monsoon: an intercomparison of CMIP5 vs. CMIP3 simulations of the late 20th century. *Climate Dynamics*, 41(9), 2711–2744. https://doi.org/10.1007/s00382-012-1607-6.

Taylor, C.M., de Jeu, R.A.M., Guichard, F., Harris, P.P. and Dorigo, W.A. (2012) Afternoon rain more likely over drier soils. *Nature*, 489, 423, 426. https://doi.org/10.1038/nature11377.

Taylor, C.M., Gounou, A., Guichard, F., Harris, P.P., Ellis, R.J., Couvreux, F. and De Kauwe, M. (2011) Frequency of Sahelian storm initiation enhanced over mesoscale soil-moisture patterns. *Nature Geoscience*, 4, 430–433. https://doi.org/10.1038/ngeo1173.

Taylor, C.M., Harris, P.P. and Parker, D.J. (2010) Impact of soil moisture on the development of a Sahelian mesoscale convective system: a case-study from the AMMA Special Observing Period. *Quarterly Journal of the Royal Meteorological Society*, 136(S1), 456–470. https://doi.org/10.1002/qj.465.

Taylor, C.M., Parker, D.J. and Harris, P.P. (2007) An observational case study of mesoscale atmospheric circulations induced by soil moisture. *Geophysical Research Letters*, 34(15), L15801. https://doi.org/10.1029/2007GL030572.

Tuinenburg, O.A. and de Vries, J.P.R. (2017) Irrigation patterns resemble ERA-Interim reanalysis soil moisture additions. *Geophysical Research Letters*, 44(20), 10341–10348. https://doi.org/10.1002/2017GL074884.

Turner, A.G. and Annamalai, H. (2012) Climate change and the south Asian summer monsoon. *Nature Climate Change*, 2, 5875–5895. https://doi.org/10.1038/nclimate1495.

Turner, A.G., Bhat, G.S., Martin, G., Parker, D.J., Taylor, C.M., Mitra, A.K., et al. (2020) Interaction of convective organisation with monsoon precipitation, atmosphere, surface and sea: the 2016 INCOMPASS field campaign in India. *Quarterly Journal of the Royal Meteorological Society*, 146(731), 2828–2852. https://doi.org/10.1002/qj.3633.

Tuttle, S. and Salvucci, G. (2016) Empirical evidence of contrasting soil moisture–precipitation feedbacks across the United States. *Science*, 352(6287), 825–828.

Wan, Z., Hook, S. and Hulley, G. (2015) *MOD11_L2 MODIS/Terra land surface temperature/emissivity 5-min L2 Swath 1km V006 [Data Set]*.

Wilson, D.R., Bushell, A.C., Kerr-Munslow, A.M., Price, J.D. and Morcrette, C.J. (2008) PC2: a prognostic cloud fraction and condensation scheme. I: Scheme description. *Quarterly Journal of the Royal Meteorological Society*, 134(637), 2093–2107. https://doi.org/10.1002/qj.333.

Xue, Y. and Dirmeyer, P.A. (2015) Land–atmosphere interactions in monsoon regimes and future prospects for enhancing prediction. *CLIVAR Exchanges*, 19, 28–30.

Zhang, J.Y., Wang, W.-C. and Wei, J.F. (2008) Assessing land–atmosphere coupling using soil moisture from the Global Land Data Assimilation System and observational precipitation. *Journal of Geophysical Research*, 113, D17119. https://doi.org/10.1029/2008JD009807.

How to cite this article: Barton EJ, Taylor CM, Parker DJ, *et al*. A case-study of land–atmosphere coupling during monsoon onset in northern India. *Q J R Meteorol Soc*. 2020;146:2891–2905. https://doi.org/10.1002/qj.3538